Nuclear Inst. and Methods in Physics Research, A 1048 (2023) 167930

Contents lists available at ScienceDirect

Nuclear Inst. and Methods in Physics Research, A

journal homepage: www.elsevier.com/locate/nima

A detection system for accurate (α, n) neutron counting measurements of low-rate (α, n) neutron sources

A. Ney [a,b,*], Y. Danon [a], M.L. Zerkle [b], P. Brain [a], D. Fritz [a], G. Siemers [a], S. Singh [a]

[a] Rensselaer Polytechnic Institute, Gaerttner LINAC Center, 3021 Tibbits Avenue, Troy, NY 12180, USA
[b] Naval Nuclear Laboratory, P.O. Box 79, West Mifflin, PA 15122, USA

ARTICLE INFO

Keywords:
(alpha, n)
Spontaneous fission
Total neutron counting
Neutron coincidence

ABSTRACT

The determination of the (α, n) neutron yield of (α, n) neutron sources with low absolute total neutron emission rates is a challenging task given the complexity of the (α, n) neutron production mechanism, experimental limitations involved with measurements of weak neutron sources, and, for sources containing special nuclear material, concurrence of the production of (α, n) and fission neutrons. However, (α, n) neutron sources are prevalent in a variety of nuclear engineering disciplines – such as nuclear fuel cycle engineering, nuclear safeguards and nonproliferation, and nuclear waste management – and as such, characterization of physical (α, n) neutron sources and accurate representation of (α, n) neutron production in neutron transport codes are critical aspects of these disciplines. In this work, a moderated ^{3}He neutron detector array with high fidelity listmode data acquisition capability was developed for measurements of low-rate (α, n) neutron sources to support (α, n) reaction nuclear data validation needs for nonproliferation applications as well as to provide experimental data for benchmarking (α, n) neutron source modeling methodologies in Monte Carlo neutron transport codes. Measurements were performed of a calibrated Eckert & Ziegler AmBe (α, n) neutron source individually and simultaneously with ^{252}Cf sources of different strengths to simulate pure (α, n) and mixed (α, n) + fission source conditions. Total neutron counting and coincidence analysis methods developed for system data analysis were applied to the measured data, and deduced (α, n) neutron yield values agreed to within 1% of the with the vendor-calibrated AmBe source (α, n) neutron yield traceable to international standards for all measurements. Total (α, n) neutron yield uncertainties for source conditions dominated by (α, n) neutron emission did not exceed 3%.

1. Introduction

The production of (α,n) neutrons via interactions of alpha particles and light nuclides is an intrinsic characteristic of many important nuclear materials. Actinides are inherently radioactive due to their high mass number and typically decay via the competing processes of alpha-decay and spontaneous fission — thus, for nuclear materials which contain both actinides and light elements, (α,n) neutron production is possible. Examples of such materials include UF_6 and U_3O_8 used in the nuclear fuel cycle as well as fresh and spent UO_2, PuO_2, and mixed-oxide (MOX) reactor fuels. The prevalence of (α,n) neutron production in principle nuclear materials drives significant interest in the modeling and characterization of (α,n) neutron sources, especially in the disciplines such as nuclear fuel cycle engineering, nuclear safeguards and non-proliferation, and nuclear waste management.

However, predicting the (α,n) neutron yield of a source analytically or computationally is difficult due to the complexity of the (α,n) neutron production mechanism. The short range of alpha particles in matter causes a strong dependence of the (α,n) neutron yield on source microscopic physical properties, such as nuclide spatial distributions in the source volume or the magnitude and distribution of any low-Z impurities in the source. For modeling purposes, such data is very difficult and expensive to obtain with sufficient accuracy. Instead, given the potential for variation in (α,n) neutron yield even among sources of the same type, size, and composition, experimental methods are best suited for determining the (α,n) neutron yield of a specific source. For measurements of (α,n) neutron production in enriched uranium compounds, which are of primary interest for end use of the system and methods developed in this work, the problem is further complicated by the fact that such materials emit a mixed field of (α,n) and neutron-induced/spontaneous fission neutrons.

Total neutron counting methods have been historically used to measure the total neutron yield of neutron-producing samples. Existing experimental systems developed for this purpose include the long counter, 4π counters, and the manganese bath system [1,2], all of which are well established technologies. Methods for correction of the total neutron yield for fission neutrons produced concurrently in

* Corresponding author.
E-mail address: Adam.Ney2@unnpp.gov (A. Ney).

https://doi.org/10.1016/j.nima.2022.167930
Received 11 July 2022; Received in revised form 23 October 2022; Accepted 9 December 2022
Available online 19 December 2022

enriched uranium compounds has been indirectly addressed by fissile material non-destructive assay (NDA) methods which also provided important historical context this work. Such systems typically consist of a large number of thermal neutron proportional counters embedded in a moderator [3], allowing for the acquisition of detected neutron time correlation data and application of coincidence analysis methods to characterize detected fission neutrons using the measured neutron pulse train.

The analysis of detected neutron pulse trains is the well-established basis for many coincidence analysis techniques and is the foundation of the work presented here. The initial identification of time intervals providing insight into source neutron characteristics was made by C.H. Vincent [4,5] who investigated the perturbation of the neutron separation spectrum (which is the basis of the methods developed in this work and referred to here as the neutron pulse time interval distribution) by the presence of detected correlated neutron groups. Over time, advanced coincidence analysis methods based on detected neutron time intervals were developed with the adoption of the Rossi-α time interval distribution, a more complex time interval distribution, which constitutes the basis of multiplicity counting techniques used for passive nuclear material non-destructive assay [6,7] as well as efficiency auto-calibration methods [8]. Given the paramount importance of these methods especially to nonproliferation applications, significant work efforts engaged in detailed studies of fission chains, neutron pulse trains, and time interval distribution characteristics [9–13] and development of advanced coincidence systems and techniques [14,15] are ongoing.

In this work, a neutron detection system and data analysis methods were developed for total and (α,n) neutron yield measurements of samples of enriched uranium compounds of known composition. The purpose of the system and method development was to provide experimental data to address (α,n) nuclear validation needs discussed in [16,17] and to support validation efforts of the in-line (α,n) neutron source sampling methodology for Monte Carlo neutron transport calculations presented in [18]. Based on these intended applications, the system was designed for measurements of sources nominally emitting 100 n/s with an α value greater than 10. An efficiency target of 50% was established for spectra of interest to facilitate high-accuracy measurements of the low-rate sources of interest in reasonable amounts of time, and a target (α,n) neutron yield accuracy of 5% was established based on validation needs. The detection system utilizes commercially-available Quaesta Instruments NPM3100U digital listmode electronics which operate as a high voltage power supply, discriminator, preamplifier, shaping amplifier, and multi-channel analyzer (MCA) in a single unit. The modules provide capability to acquire high-fidelity neutron listmode data containing every neutron detection event with an associated pulse height and timestamp for each ^{3}He neutron detector in the system. Total neutron counting and novel coincidence data analysis methods were developed to determine the (α,n) neutron yield from measured listmode data.

2. Neutron detector system

2.1. System design

The experimental challenges involved in measurements of the (α,n) neutron yield of low-rate neutron sources led to a number of critical design considerations:

1. Absolute neutron detection efficiency for neutron spectra of interest
2. Neutron background sensitivity
3. Gamma ray sensitivity
4. System response sensitivity to neutron energy
5. System coincidence capability

Statistically accurate measurements of low-rate neutron sources are accelerated for systems with high absolute neutron detection efficiencies and low intrinsic and extrinsic background sensitivity. The target of 50% efficiency for (α,n) and fission neutron spectra of interest was considered a reasonably achievable requirement within strict and limiting system size constraints (based on measurement facility limitations) while balancing the need to perform high-accuracy measurements in a reasonable amount of time. Low sensitivity to gamma rays was required to ensure that the detection of gamma rays emitted through decay or nuclear reaction processes in the source do not confound measurements. For total neutron counting analysis, the system response must have low sensitivity to source neutron kinetic energy imposed either through geometric properties of the system or artificially via analytical methods. Coincidence capability was necessary to account for the fission neutron contribution in measured data.

Based on these considerations, a high-density polyethylene (HDPE) moderated ^{3}He neutron detector array was chosen as the conceptual design for the detector system. This concept was based on the designs of typical neutron multiplicity counters and was selected based on confidence in the ability to design a system which met the efficiency and sensitivity requirements necessary for measurements of low-rate neutron sources and which could supply raw measured data useful for both total neutron counting and coincidence analysis. Consideration was given to the use of other types of thermal neutron detectors which employ different neutron converters — for example, BF_3 proportional counters, Li-glass scintillation detectors, or solid-state detectors which utilize the ^{10}B(n, α) or ^{6}Li(n, α) conversion reactions. However,^{3}He detectors were selected despite their high cost for a number of reasons:

1. ^{3}He detectors have superior thermal neutron detection efficiency given that:
   (a) The ^{3}He(n,p) thermal neutron cross section is larger than that of the ^{10}B(n, α) or ^{6}Li(n, α) reactions [19]
   (b) ^{10}B and ^{6}Li are not the dominant isotopes existing in natural boron and lithium, limiting intrinsic efficiency without enrichment
   (c) BF_3 gas is poisonous and therefore is typically underpressurized in proportional counters, whereas ^{3}He gas can be pressurized to increase intrinsic efficiency
2. The gamma ray sensitivity of ^{3}He detectors is lower than that of BF_3 and Li-glass detectors
3. The electronics required for operation of gas-filled detectors are simpler than the photomultiplier tube electronics associated with Li-glass scintillation detectors, and this benefit scales further in favor of ^{3}He detectors with the implementation of many discrete detectors required for coincidence analysis
4. Solid state detectors are size-limited and therefore require many individual detectors to achieve the same efficiency of a much larger ^{3}He proportional counter

Additional details on the concept generation, concept selection, and system design processes are presented in [20].

The system geometry was designed using MCNP-6.2 [21] Monte Carlo neutron transport simulations with ENDF/B-VIII.0 nuclear data [19]. Design iterations were compared largely based on the computed absolute neutron detection efficiency for a set of spontaneous fission and (α,n) sources in addition to estimated cost and adherance with laboratory physical constraints. Computer-aided design (CAD) assemblies of the final detector system design are shown in Figs. 1 (trimetric view), 2 (section view), and 3 (top view). A photograph of the as-built detector system is shown in Fig. 4.

The design consists of 96 LND 252330 ^{3}He proportional counters with a fill gas pressure of 5 atm. Properties and operating parameters of the LND 252330 ^{3}He detectors are given in Table 1. The detectors are embedded in a 24" × 24" cylindrical stack of HDPE plates ($\bar{\rho}$ = 0.953

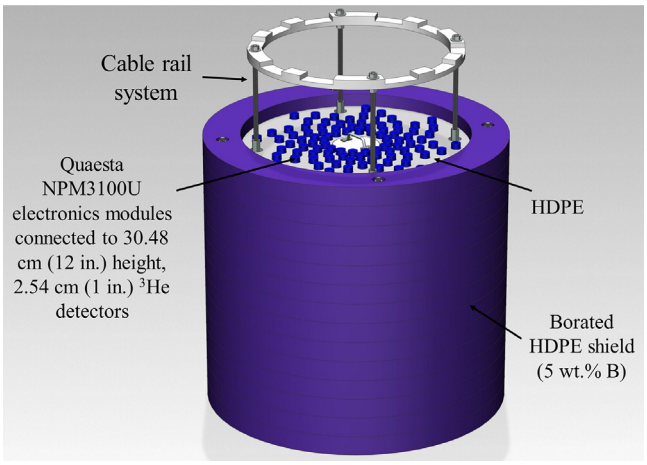

Fig. 1. Trimetric view of the final neutron detector system computer-aided design (CAD) assembly. Overall dimensions: 101.6 cm (40 in.) height, 81.28 cm (32 in.) diameter.

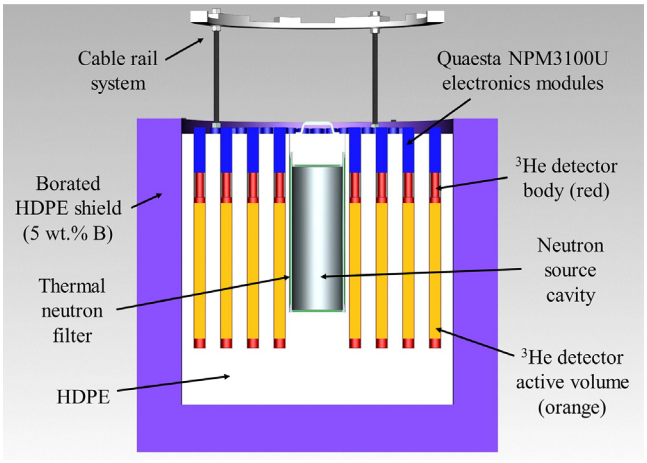

Fig. 2. Section view of the final neutron detector system computer-aided design (CAD) assembly.

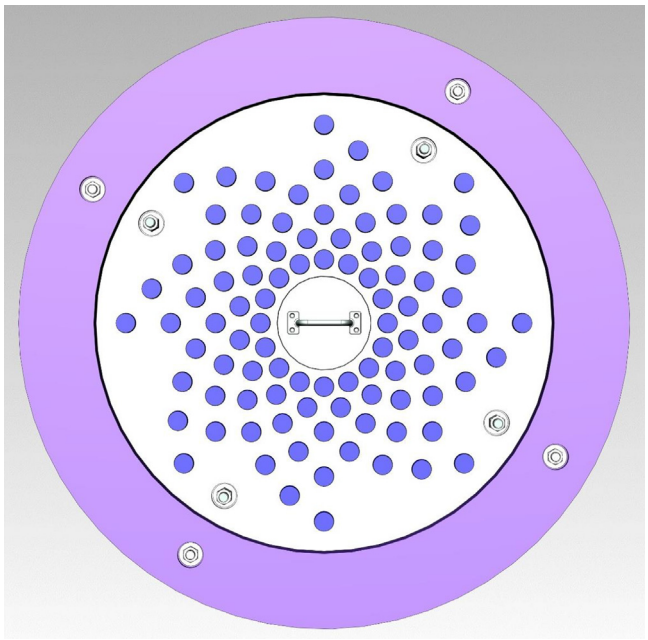

Fig. 3. Top view of the final neutron detector system computer-aided design (CAD) assembly.

Fig. 4. Photograph of the as-built detector system. The system was constructed on a cart with wheels for ease of maneuverability and can pass through doors wider than 81.28 cm (32 in.).

g/cm^3), aligned with the HDPE axial midplane, and are arranged in 7 rings. The detector rings are concentric with the HDPE cylinder and are located at radial locations ranging from 8.5 cm (ring 1) to 26.5 cm (ring 7) with uniform radial spacing of 3 cm. There are 16 ^{3}He detectors contained in rings 1–5 and 8 detectors contained in rings 6 and 7.

To perform a measurement, the neutron source of interest is placed in the central cavity of the detector system and is aligned with the axial and radial center of the HDPE cylinder. An HDPE plug is inserted at the top of the cavity, and a rail apparatus stands above the HDPE cylinder to support the electronics cables and reduce fatigue where the cables connect to the detector electronics.

The primary figure of merit used in determining the system dimensions as well as the ^{3}He detector size, fill gas pressure, and spatial distribution during the design process was the system absolute neutron detection efficiency for the ^{252}Cf spontaneous fission prompt fission neutron energy spectrum (PFNS). The primary design goal was to maximize the system efficiency while remaining within the design space defined by the project sponsor technical specifications and target cost. For example, the design basis neutron source characteristics defined by the sponsor ($S \approx 100$ n/s, $\alpha > 10$) called for a maximization of the size and number of ^{3}He detectors used, but these characteristics were constrained by both cost limitations as well as sponsor technical specifications (e.g. a maximum system width of 36 in., minimum source

Table 1
LND 252330 ^{3}He detector properties and operating parameters.

Property	Value
Fill gas	^{3}He, CO_2
^{3}He partial pressure [atm]	4.95
CO_2 partial pressure [atm]	0.05
Total gas pressure [atm]	5.00
Recommended operating voltage [V]	981
Operating voltage range [V]	850–1100
Maximum length [inch/mm]	15.23/386.4
Maximum diameter [inch/mm]	1.0/25.4
Active length [inch/mm]	12.0/304.8
Active diameter [inch/mm]	0.96/24.38
Active volume [cm^3]	142.26
Anode wire diameter [inch/mm]	0.002/0.00508
Anode material	Stainless steel
Cathode material	Stainless steel
Connector	HN

cavity diameter of 4.5 in.). Sensitivity studies were performed, adjusting the system moderator diameter and height,^{3}He detector size and layout, and cavity diameter, to maximize the system efficiency while minimizing the project cost. The amount of information embedded in collected data was also a consideration in designing the detector spatial layout — for example, despite detector rings 6 and 7 contributing very little to the overall absolute neutron detection efficiency of the system, these rings were implemented for purposes of obtaining coarse neutron energy spectrum information.

In addition to the use of a large number of ^{3}He detectors for increased detection efficiency and coincidence analysis capability, two aspects of the detector system were designed specifically to enhance measurement capabilities for low-rate (α,n) neutron sources. First, the sample cavity is fully lined with a 1 mm-thick aluminum-housed cadmium thermal neutron filter. The filter significantly reduces the probability of backscattered thermal neutrons returning from the moderator to the sample which have the potential to cause secondary neutron-induced fission. Evaluation of various thermal neutron filter designs were evaluated using Monte Carlo simulations of physical neutron-producing samples to determine the sensitivity of the neutron-induced fission rate in a given sample to the cadmium layout and thickness. The intention of these studies was to balance the goals of minimizing the neutron-induced fission rate and minimizing the amount of cadmium used given its hazardous nature — the studies showed that a 1 mm-thick filter was most suitable given these competing objectives.

Additionally, the HDPE cylinder is surrounded on the bottom and sides with a 4 inch thick, 5 wt% borated HDPE shield. The shield was implemented with two primary purposes — the reduction of neutron leakage from the system, which may lead to source-dependent neutron background (room return) and perturbation of the count rates in the outermost detector rings, as well as the reduction of source-independent neutron background which has the same effect. The determination of the shield thickness was performed using Monte Carlo simulations of various neutron spectra with a thick concrete wall modeled surrounding the system on all sides. Sensitivity of the total room return count rate on shield thickness was performed, where it was found that beyond a thickness of 4 inches the effectiveness of the shield in reducing room return rapidly diminishes. Note that source-dependent neutron background was considered more of a concern in the system design than source-independent neutron background (especially cosmic neutron background, which is exceptionally important for low rate neutron source measurements). This is because the facility in which the system will be used in perpetuity is considered to be adequately shielded from cosmic neutron background.

2.2. Neutronics properties

Neutronics properties critical to system performance for low-rate (α,n) neutron source measurements — namely, the absolute neutron detection efficiency ε and average neutron dieaway time τ_s — were evaluated throughout the design process using MCNP-6.2 neutron transport calculations. Note that while the average neutron dieaway time was tracked throughout this process, it was not emphasized as heavily as detection efficiency in evaluation of design iterations. The average neutron dieaway time was determined using MCNP-6.2 PTRAC output which provides event-based particle track information for each neutron transported. Using this output, the average neutron dieaway time was computed by taking the arithmetic mean of the time to detection for all detected neutrons.

The neutronics properties for the final system design are summarized in Table 2 for a number of relevant neutron sources. Note that the uncertainties given for the efficiency values represent 1-sigma MCNP statistical uncertainties. These spectra were obtained in a number of ways — the (α,n) spectra were all computed using SOURCES 4C [22] with PuO_2 and AmBe source compositions obtained from [18], a PuBe source composition obtained from [22], and a UO_2 source composition corresponding to a nominal source density of 9.95 g/cm and ^{235}U enrichment of 5 wt%. The fission spectra utilized were the ENDF/B-VIII.0 evaluations of the corresponding nuclide prompt fission neutron spectra. The calculations found that the system met the target efficiency of roughly 50% for the ^{252}Cf spontaneous fission PFNS and that the neutron dieaway times for all spectra simulated were less than 44 μs.

2.3. Detector electronics

The detector system utilizes 96 Quaesta NPM3100U digital electronics modules, one for each ^{3}He detector. The modules act as a high voltage power supply, preamplifier, shaping amplifier, discriminator, multi-channel analyzer (MCA), and listmode data acquisition module and connect directly to the ^{3}He detector high-voltage type-N (HN) connectors. The selection of the Quaesta units over other modules commonly used in similar applications, such as those offered by PDT or AMPTEK, was motivated by the fact that the modules provide all components necessary for detector operation and data collection in one unit, allowing for a very clean and simple electronics setup. Additionally, the fact that the modules connect directly to the ^{3}He detector HN connectors minimizes signal noise. The computer interface for detector operation and data collection with the modules was also seamless out-of-the-box without additional development.

Each module has three connections — universal serial bus (USB), transistor–transistor logic (TTL)-in, and TTL-out. The modules are connected to a hub rack (shown in Fig. 6) via a USB cable and an subminiature version A (SMA) cable connected to the TTL-in connector. Photographs of an NPM3100U module connected to a ^{3}He detector are shown in Fig. 5.

The USB connection is used for device serial communication and data acquisition for each ^{3}He detector. Through serial commands, an experimenter may control the power supply (set and read high voltage and limit maximum applied voltage), configure the MCA parameters (gain, lower and upper discriminators, and bin structure), and acquire listmode data. The SMA connection is used for onboard clock synchronization of all 96 modules in the system. An additional synchronization NPM3100U unit is contained in the USB/SMA hub rack and is configured to send TTL pulses, split out to all 96 detector modules via the SMA hub, at a rate of 2 Hz. The receipt of these TTL pulses by all detector units causes synchronization of the clocks, ensuring that the timestamps of events in each detector are accurate and synchronized to a resolution of 1 μs. The 1 μs resolution was considered more than adequate given the fact that the time interval distributions constructed for analysis (see Sections 3.4.2 and 3.4.3) are aggregated with bin

Table 2
System neutronics properties for various (α,n) and fission neutron sources computed with MCNP-6.2. Transport calculations utilized (α,n) neutron energy spectra computed using SOURCES-4C [22] and ENDF/B-VIII.0 pointwise evaluations for prompt fission neutron energy spectra.

Neutron source	Absolute neutron detection efficiency [%]	Average neutron dieaway time [μs]
AmBe (α,n)	38.244 ± (0.008)	43.5 ± 0.2
PuBe (α,n)	38.821 ± (0.008)	43.2 ± 0.2
UO_2 (α,n)	49.355 ± (0.005)	39.8 ± 0.2
PuO_2 (α,n)	48.049 ± (0.005)	40.1 ± 0.2
^{235}U(n,f)	50.635 ± (0.005)	38.0 ± 0.1
^{239}Pu(n,f)	50.077 ± (0.005)	38.3 ± 0.2
^{252}Cf s.f.	50.079 ± (0.005)	38.2 ± 0.2

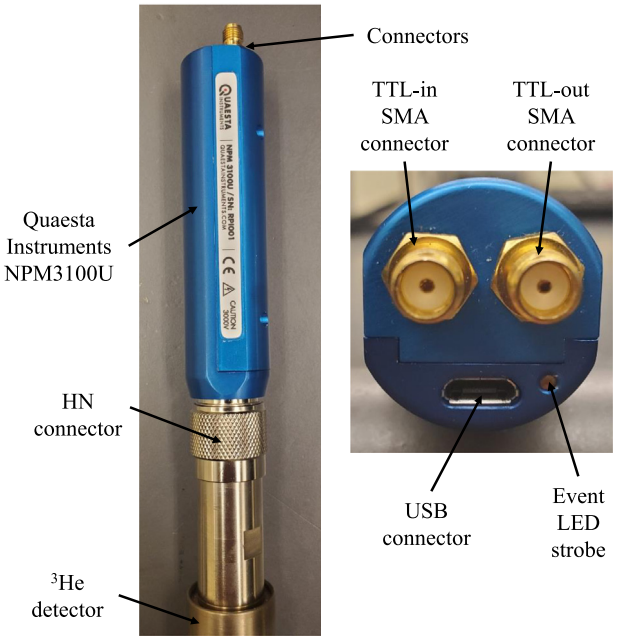

Fig. 5. Photograph of a Quaesta NPM3100U module connected to a ^{3}He detector (left) and the module USB, TTL-in, and TTL-out connectors (right).

Table 3
Nominal operating parameter settings for the LND ^{3}He detectors via the Quaesta Instruments NPM3100U digital electronics modules.

Parameter	Setting
Nominal applied voltage	950 V
Gain	6.0
MCA size	64 bins
Lower-level discriminator	10
Upper-level discriminator	63

widths no less than 10 μs. Nominal operating parameters for the ^{3}He and NPM3100U module pairs are given in Table 3.

Neutron detection event pulse shaping is performed using a hardware-set 10 μs pulse shaping constant, and multiple pulses cannot be registered within an electronic lockout time of 100 μs. This lockout time, which is quite long in comparison to typical neutron dieaway times for spectra of interest in the system, was selected in order to ensure full charge collection in the ^{3}He detectors and to simplify dead-time corrections of measured count rates. Utilizing a neutron pulse train simulation code developed in-house as part of this work, calculations with both design basis source conditions and source conditions on the order of the sources utilized in the method validation measurements (see Section 5) found that the correlated neutron loss rate in the system is approximately 1% with a 100 μs lockout time for a mix of AmBe (α,n) and ^{252}Cf s.f. neutrons.

To ensure that the ^{3}He detectors operate with matched efficiencies in each ring, a voltage calibration process is performed prior to measurements. In this process, which is automated and performed using the data acquisition software developed for the system (see Section 2.4), the voltage applied to each detector is adjusted in order to align the peaks of the measured pulse height distributions of all detectors to the same MCA bin. This normalizes the impact of the lower and upper level discriminator settings across all detectors and in turn matches the efficiencies. Fig. 7 shows the ring 1 ^{3}He detector count rate and pulse height distribution alignment from a measurement of a ^{252}Cf neutron sources.

The Quaesta electronics can be utilized for either integral or differential counting measurements. For integral measurements, the number of counts, count rate, and pulse height distribution are retained in the module memory and can be queried by a user. For differential measurements, the user can obtain event-by-event listmode data over a given period of data acquisition. An example of the ASCII listmode data format is given in Listing 1.

Listing 1: Example of the raw ASCII listmode data format collected by the Quaesta NPM3100U modules.

```
1,1,39,0.028653600
1,1,40,0.327165000
2,1,00,0.372717600
2,1,00,0.872716500
1,1,39,1.069923100
```

Each line corresponds to a pulse received by the module and is a four-element CSV array describing the event. Moving left to right, the elements indicate:

1. The type of pulse received (1 = neutron detection event, 2 = time synchronization pulse)
2. The module identification number (1 in the example)
3. The MCA bin number corresponding to the event pulse height (note that for synchronization pulses, this value is 0)
4. The time [s] at which the event occurred

The collection of listmode detection event data for each individual detector gives an experimenter ultimate flexibility in data analysis, allowing for a measurement to be analyzed in a variety of ways with different analysis parameters — for example, a set of raw data can be analyzed using a number of total neutron counting and coincidence algorithms with parameters tuned in post-processing instead of preset in hardware. Furthermore, given that the measured data has both temporal and spatial dimensionality, the amount of information embedded in the data is extensive, making it an excellent testbed for exploratory data analysis and the development of novel algorithms. The collection of each detector's pulse height spectrum can also be leveraged to monitor the performance and calibration of each ^{3}He detector as a function of time throughout an experiment.

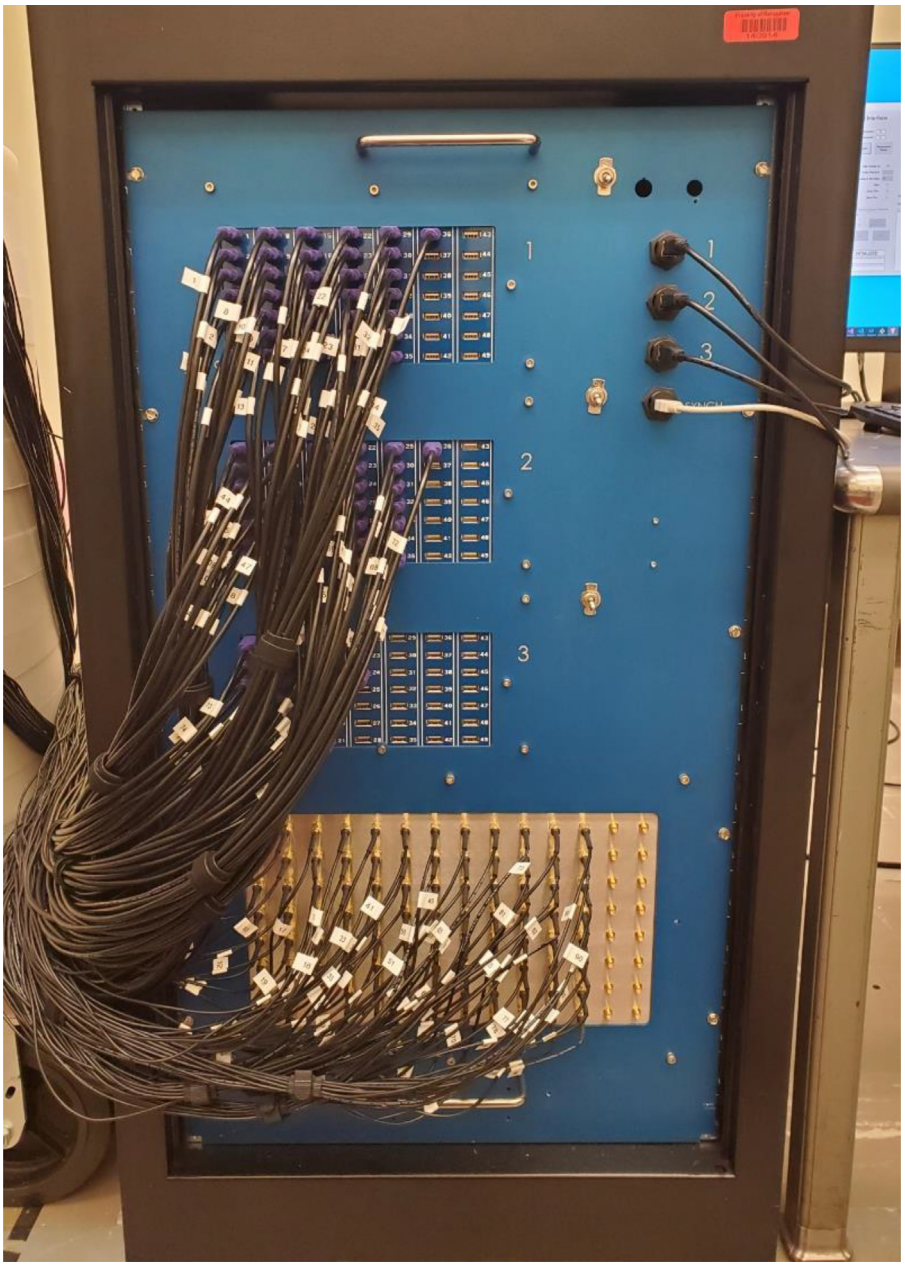

Fig. 6. Photograph of the USB/SMA hub rack containing three 49-port USB hubs and one 112-port SMA hub. Each of the four hubs is connected to the data acquisition computer via a USB cable.

2.4. Data acquisition software

The data acquisition software for the detector system was developed in-house as part of this work and was written in VB.NET. VB.NET was chosen for ease of use in developing a feature-rich graphical user interface (GUI) for the software, which was preferred to a command line interface and provides added flexibility for data visualization and system health monitoring throughout measurements. Using the software, an experimenter can accomplish four primary tasks — hardware configuration, measurement configuration and control, real-time data display, and the reading and writing of listmode data.

To perform a measurement, the software first establishes serial connection to all 96 NPM3100U detector electronics modules and the time synchronization module contained in the USB/SMA hub rack. Once connection is established, the user may use the GUI or preloaded configuration files to set the detector applied voltage and the MCA gain, lower- and upper-level discriminators, and bin structure. Following hardware configuration, the user can use the GUI to set the measurement parameters (name, save file location, number of cycles, and cycle length) and start data acquisition.

During a measurement, raw ASCII listmode data for each of the 96 ^{3}He detectors in the system is continuously read from each detector's associated serial port buffer. The data is processed for each ^{3}He detector on-the-fly to aggregate the cumulative number of counts, count rate, and pulse height distribution as well as the count rate and pulse height distribution centroid for each measurement cycle used for monitoring hardware stability. This data is retained in memory and may be displayed in real-time by an experimenter in the software interface throughout a measurement. The raw listmode data for each detector is periodically written to a text file corresponding to the detector and cycle. The implementations of the data read/write algorithms are multi-threaded, maximizing utilization of computing power and increasing the maximum event rate which can be handled by the system. As a result, the maximum handled event rate is a function of the CPU

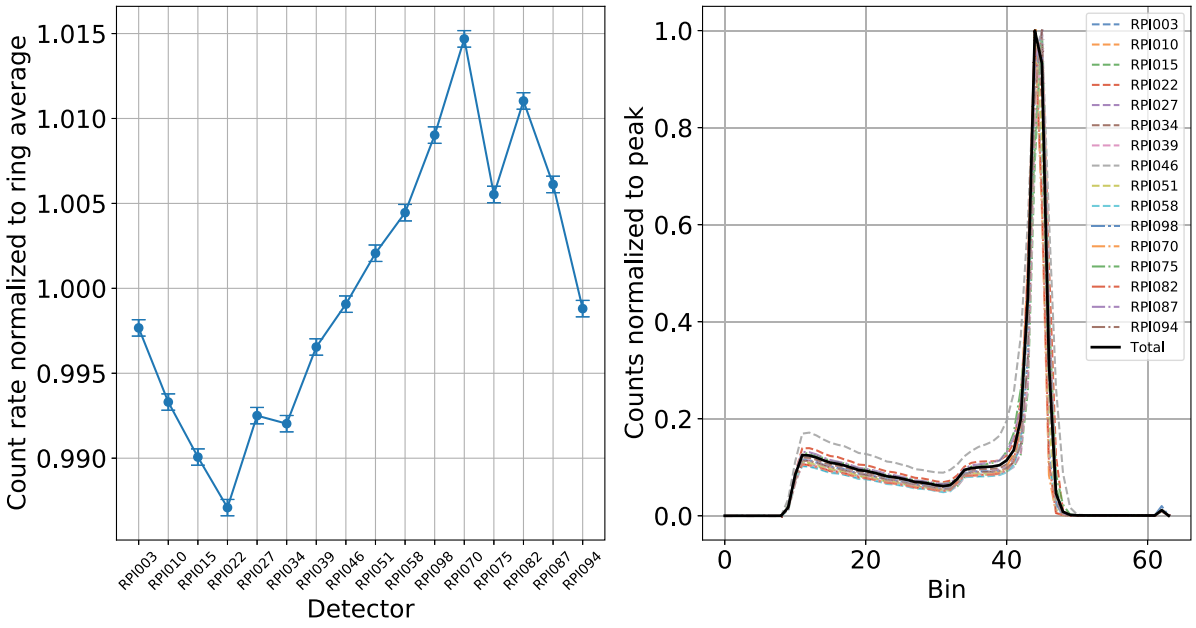

Fig. 7. Measured count rate and pulse height distribution alignment for the 16 ^{3}He detectors in ring 3 of the detector system obtained from a ^{252}Cf source measurement. The count rates are shown to fluctuate within roughly ± 1.5% of the average count rate in the ring. The oscillatory trend in the count rate is due to slight misalignment of the ^{252}Cf in the source cavity during the measurement.

resources of the data acquisition computer. For scale, testing using the built-in pulse generators in the Quaesta electronics modules has shown that the software maintains stability up to rates of 1000 Hz per ^{3}He detector with a 3.60 GHz Intel Core i9-9900k CPU.

3. Data analysis methods

3.1. Method inputs

Given the detector system design, electronics configuration, and listmode data format, the raw data collected for each of the 96 ^{3}He detector is extremely high fidelity. Possessing both spatial and temporal dimensionality, the raw listmode data may be aggregated and analyzed in any number of ways and provides an experimenter with the ability to investigate spatial detection information and/or neutron time correlation. Prior to data analysis, raw measured data is aggregated into three formats: the total system neutron count rate, the system response function which possesses spatial dependence, and the system time interval distribution which possesses time dependence.

The background- and deadtime-corrected count rate for the k^{th} detector in ring j is denoted $r_{j,k}$. Details on background and deadtime correction methods with associated uncertainty quantification applied to the method validation measurement data presented in Section 5 are discussed in [20]. Note that for these measurements, which involved neutron sources with higher yields that the design basis source conditions, the maximum total ((α,n) + fission neutron) deadtime loss predicted using the correction method for a given ^{3}He detector was 1.6%.

The system total count rate r_{tot} is obtained by summing the corrected count rates for all 96 ^{3}He detectors,

$$r_{tot} = \sum_{j=1}^{7} \sum_{k=1}^{n_j} r_{j,k}, \tag{1}$$

where n_j is the number of detectors in ring j,

$$n_j = \begin{cases} 16 & 1 \le j \le 5 \\ 8 & \text{otherwise.} \end{cases} \tag{2}$$

The system response function, a seven-element vector $\vec{R}$ where the jth element is the system response in ring j, is the average neutron count rate per detector in each of the seven detector rings,

$$R_j = \frac{1}{n_j} \sum_{k=1}^{n_j} r_{j,k} \qquad j = 1, 2, \ldots, 7. \tag{3}$$

The system time interval distribution is the histogram of time intervals between consecutive neutron detection events in the detector system. This is computed by first merging and sorting the listmode data by timestamp for all 96 ^{3}He detectors. The time intervals between each consecutive timestamp are computed and binned on a bin structure defined by the experimenter. This process is repeated for each cycle and the results are aggregated.

3.2. Total neutron counting

A detector weighting method was developed for total neutron counting analysis of measured data. The purpose of the method is to obtain the total (e.g. (α,n) + fission) neutron yield of a measured neutron source. In the method, it is assumed that the source total neutron yield, S, is the linear combination of the corresponding measured system response function, $\vec{R}$, and a set of seven detector weights, $\vec{w}$, each weight corresponding to a specific detector ring,

$$S = \sum_{j=1}^{7} w_j R_j. \tag{4}$$

The detector weights are assumed to be universal — that is, the total neutron yield of any source may be obtained applying the weights to the corresponding measured response function. As a result, the weighting model given in Eq. (4) may be extended to a set of n response functions computed using MCNP-6.2 [21] transport simulations of n monoenergetic neutron sources. Under the assumption of universality, a system of n linear equations may be formed using the n simulated monoenergetic response functions, and the system may be combined to form a matrix equation,

$$\boldsymbol{R_m}\vec{w} = \vec{S}, \tag{5}$$

where $\boldsymbol{R_m}$ is an $n \times 7$ response matrix containing the simulated response values for each of the n monoenergetic neutron sources in each of the

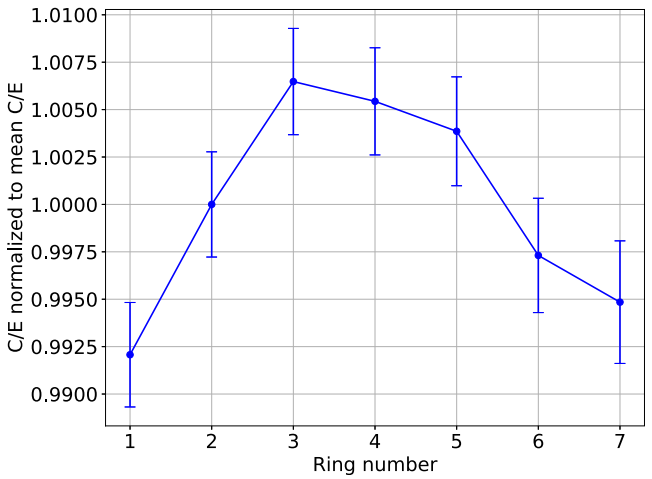

Fig. 8. C/E ratio of measured and simulated response functions for a ^{252}Cf spontaneous fission neutron source as a function of ^{3}He detector ring number. The simulation shows excellent accuracy with C/E magnitudes of less than 1% for all rings.

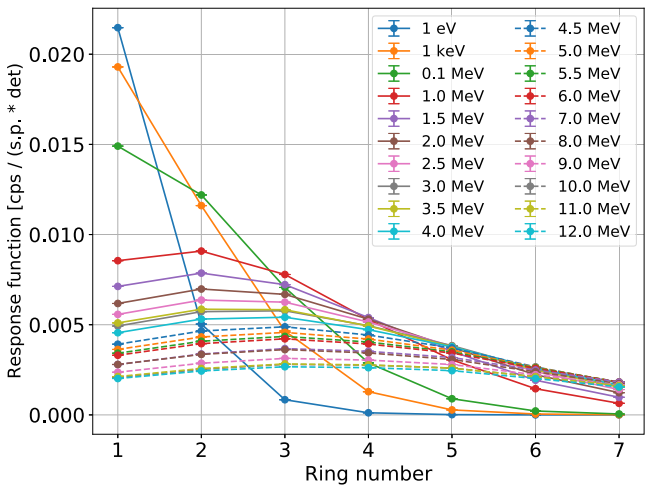

Fig. 9. Simulated response functions for the selected weighting energy grid.

seven detector rings. The neutron yield vector, $\vec{S}$, is a vector of all ones due to MCNP tally normalization per source neutron. For the detector weighting method, n is typically greater than 7 and the weights must therefore be estimated by solving the matrix equation using linear least squares regression,

$$w \approx \hat{w} = \left(\boldsymbol{R}_{\boldsymbol{m}}^{T}\boldsymbol{R}_{\boldsymbol{m}}\right)^{-1}\boldsymbol{R}_{\boldsymbol{m}}^{T}\vec{S}. \tag{6}$$

To reduce the sensitivity of the weight calculation to the statistical uncertainty of the simulated response matrix, Eq. (6) is solved m times each with a sampled statistical realization of the response matrix. The statistical realizations are generated by sampling each simulated response value on a Gaussian distribution with a mean equal to the computed value and a standard deviation equal to the computed value's statistical uncertainty. The final weights for each ring are then taken as the average of the m weight values computed in this process,

$$w_j = \frac{1}{m}\sum_{i=1}^{m} w_j^{(i)} \qquad j = 1, 2, \ldots, 7. \tag{7}$$

Once the weights are determined, they may be applied to any measured response function via Eq. (4) in order to determine the total neutron yield of the measured source. The statistical uncertainty of the computed total neutron yield is obtained by applying general uncorrelated uncertainty propagation to Eq. (4). In this case, the weight uncertainty is not propagated as statistical uncertainty and is instead included as a component of the method systematic uncertainty, discussed further in Section 3.3. This uncertainty quantification process is detailed in [20].

Given that the weighting method relies heavily on the use of simulations, evaluation of the accuracy of the MCNP model used to generate the response matrix was of critical importance. To do this, a comparison of the response functions measured and simulated for a ^{252}Cf spontaneous fission neutron source was performed. The C/E values for the measured and simulated response functions were computed for each ring, normalized by the average C/E value, and plotted for comparison as a function of ring number. This is shown in Fig. 8. Note that ^{252}Cf was chosen for this comparison because measurement data was available and the ^{252}Cf spontaneous fission PFNS is a standard, eliminating the neutron energy spectrum as a factor which could contribute to differences in response function shape.

Fig. 8 shows excellent agreement between the shapes of the measured and simulated response functions for a ^{252}Cf neutron source. This instilled confidence in the use of the developed MCNP model for generation of response matrices used in the detector weighting method.

Table 4
Weights computed using the detector weighting method with the selected weighting energy grid used for validation measurement analysis.

Ring number	Weight
1	−4.19
2	391.78
3	−1415.36
4	2980.09
5	−2591.49
6	−439.40
7	2078.91

3.3. Weighting method parameters

To compute the detector weights, the following weighting energy grid was utilized for the simulated monoenergetic neutron source response functions: 1 eV, 1 keV, and 0.1, 1, 1.5, 2, 2.5, 3, 3.5, 4, 4.5, 5, 5.5, 6, 7, 8, 9, 10, 11, and 12 MeV. This grid was chosen based on performance testing with simulated response functions of (α,n) and fission neutron energy spectra of interest and was advised by the fact that neutron energies spanning 1 eV to 12 MeV cover the range of typical spectra. Additionally, simulated response functions for neutron energies greater than 12 MeV were found to be very similar in both shape and magnitude and were therefore omitted from use to avoid overfitting of the weight model and to improve weight generalization. The simulated responses for this energy grid are shown in Fig. 9.

Using this energy grid and the corresponding simulated response matrix, the detector weights given in Table 4 were computed.

To estimate the systematic uncertainty of a total neutron yield value computed using the detector weighting method, the weights given in Table 4 were applied to simulated response functions for eight (α,n) and fission neutron energy spectra across the domain of interest for this work. Because the simulated response functions were computed using MCNP-6.2 normalized tallies, the expected neutron yield for all simulated sources was 1. The systematic uncertainty was taken as one half of the maximum absolute error of the seven computed neutron yields. The results of this analysis are shown in Table 5, where the systematic uncertainty was taken as 1.35%.

3.4. Coincidence analysis

In this work, two neutron coincidence analysis methods were developed which utilize the measured time interval distribution discussed in Section 3.1. These methods are referred to as the fission source

Table 5
Detector weighting energy grid and weight performance on simulated neutron source response functions. Transport calculations utilized (α,n) neutron energy spectra computed using SOURCES-4C [22] and ENDF/B-VIII.0 pointwise evaluations for prompt fission neutron energy spectra.

Neutron source	Computed neutron yield	Absolute error
Energy grid average	1.0282	0.0282
AmBe (α,n)	1.0182	0.0182
PuBe (α,n)	1.0248	0.0248
UO_2 (α,n)	0.9731	**0.0269**
PuO_2 (α,n)	0.9832	0.0168
^{252}Cf s.f.	1.0095	0.0095
^{238}U(n,f)	1.0228	0.0228
^{239}Pu(n,f)	1.0155	0.0155

time interval distribution analysis (FTIDA) method and the mixed (α,n) + fission neutron source time interval distribution analysis (MTIDA) method. The purpose of the FTIDA method is to auto-calibrate the absolute fission neutron detection efficiency for a measured fission neutron source, and the purpose of the MTIDA method is to isolate the components of the total measured count rate due to (α,n) and fission neutrons. The developed coincidence methods relate the structure and features of measured time interval distributions to neutron detection theory in order to accomplish their associated objectives.

3.4.1. Theory

For a random, uncorrelated neutron source, the probability density function of time intervals (Δt) between consecutive neutron detection events,

$$f_{\Delta T}(\Delta t) = re^{-r\Delta t}, \tag{8}$$

is an exponential distribution dependent on the average neutron detection rate r [23]. For correlated neutron sources, such as pure fission and mixed (α,n) + fission neutron sources, the time interval distribution is multi-exponential. This is due to the time correlation of the detected fission neutron multiplets which result in an increased number of observed short time intervals. For thermal neutron detection systems the distribution has a double exponential form, and for epithermal neutron detection systems the distribution is a higher-order exponential function due to multiple slowing down modes existing at short detection times.

To demonstrate the dependence of measured time interval distribution structure on neutron source characteristics, the time interval distribution obtained from the measurement of an Eckert & Ziegler ^{252}Cf spontaneous fission neutron source is shown in Fig. 10 plotted on a semilog scale. This measurement was performed for 48 h and was a component of the set of method validation measurements discussed in detail in Section 5. The distribution is separated into two distinct regions: region 1, which contains time intervals between uncorrelated neutrons, and region 2, which contains time intervals between correlated neutrons. Note that region 1 follows the single exponential distribution theory given for uncorrelated neutron detection in Eq. (8).

For measurements of a pure fission neutron source, uncorrelated time intervals arise from the consecutive detection of:

1. Two fission neutrons from different fission events
2. Two background neutrons
3. One fission neutron and one background neutron

Correlated time intervals arise only from the consecutive detection of two fission neutrons from the same fission event.

Similarly for mixed (α,n) + fission neutron sources, the measured time interval distribution obtained from the measurement of Eckert & Ziegler AmBe (α,n) and ^{252}Cf s.f. neutron sources simultaneously is shown in Fig. 11, plotted on a semilog scale. This measurement was performed for 28.75 h and was another component of the method validation measurement set, discussed in detail in Section 5. The shape of the measured time interval distribution is similar to that measured for a pure fission neutron source and is partitioned in the same way. However, neutron contributions to the uncorrelated time interval region are different. For measurements of a mixed (α,n) + fission neutron source, uncorrelated time intervals arise from the detection of:

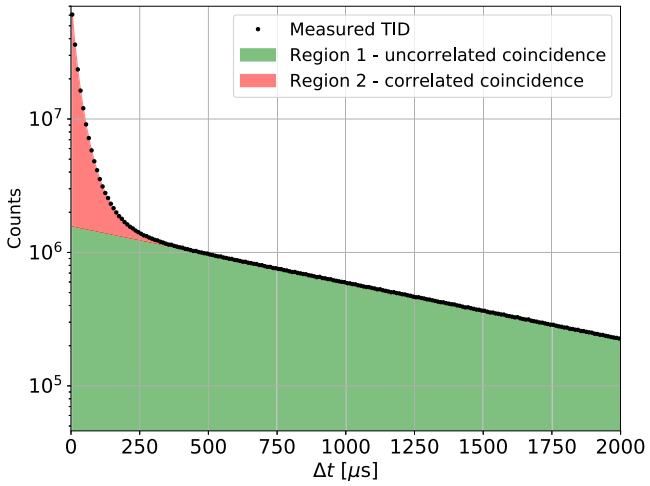

Fig. 10. Time interval distribution obtained from a measurement of a ^{252}Cf spontaneous fission neutron source.

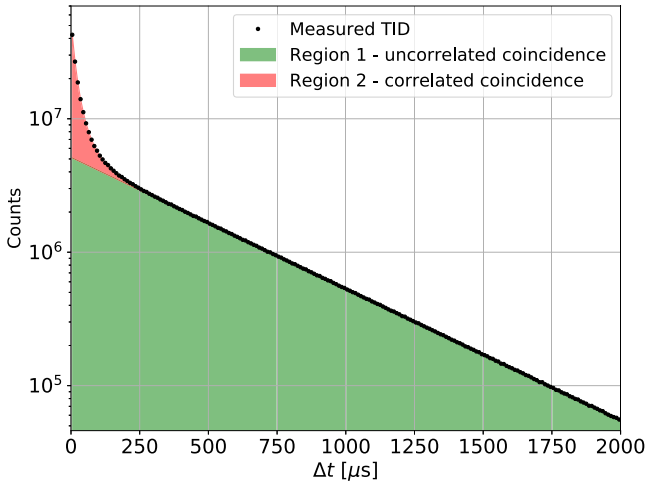

Fig. 11. Time interval distribution obtained from a measurement of an AmBe (α,n) neutron source + a ^{252}Cf spontaneous fission neutron source.

1. Two fission neutrons from different fission events
2. Two (α, n) neutrons
3. Two background neutrons
4. One fission neutron and one (α,n) neutron
5. One fission neutron and one background neutron
6. One (α,n) neutron and one background neutron

The constituents of region 2, however, are the same as for a pure fission source — correlated time intervals arise only from the consecutive detection of two fission neutrons from the same fission event.

Relating the structure of the measured time interval distributions — namely, the integral of region 2 (e.g. number of correlated time intervals) and the slope of region 1 (e.g. the uncorrelated neutron count rate) to neutron detection theory is the basis of the FTIDA and MTIDA methods. The principal detection theory utilized in the FTIDA and MTIDA methods is fission neutron multiplet detection theory,

specifically the probability to detect i neutrons from a fission event, P_i [8],

$$P_i = \sum_{\nu=i}^{\infty} \binom{\nu}{i} \varepsilon_f^i \left(1-\varepsilon_f\right)^{\nu-i} P(\nu), \tag{9}$$

where $P(\nu)$ is the effective prompt fission neutron multiplicity distribution for the fissioning nuclide(s) in the neutron source. This distribution is a discrete probability distribution defining the probability that ν neutrons are emitted in a fission event. The average of this distribution, $\bar{\nu}$, is the average number of fission neutrons emitted per fission,

$$\bar{\nu} = \sum_{\nu=1}^{\infty} \nu P(\nu). \tag{10}$$

The development of the FTIDA method for pure fission neutron source absolute detection efficiency auto-calibration and the MTIDA method for (α,n) and fission neutron count rate separation are based on the qualitative time interval distribution structure theory and the neutron detection theory discussed here. The FTIDA method is discussed in detail in Section 3.4.2, and the MTIDA method is discussed in detail in Section 3.4.3.

3.4.2. The FTIDA method

The purpose of the FTIDA method is to auto-calibrate the absolute fission neutron detection efficiency for a pure fission neutron source. In measurements of a pure fission neutron source, the total count rate measured with the detector system, r_{tot}, is the sum of the fission and background neutron count rates r_f and r_b,

$$r_{tot} = r_f + r_b. \tag{11}$$

The background count rate is the total count rate computed using Eq. (1) for a separate background measurement with no neutron sources in the detector system.

The fission neutron count rate can be decomposed as the sum of two components: one component representing the count rate of fission neutrons contributing to time intervals in region 1 of the time interval distribution, r_{f1}, and another component representing the count rate of fission neutrons contributing to time intervals in region 2, r_{f2},

$$r_f = r_{f1} + r_{f2}. \tag{12}$$

The uncorrelated neutron count rate, r_1, is the sum of the background neutron count rate and the count rate of fission neutrons contributing to region 1,

$$r_1 = r_{f1} + r_b = \left(r_f - r_{f2}\right) + r_b, \tag{13}$$

where the value of r_1 is obtained from the measured time interval distribution by fitting a single exponential function to region 1.

The count rate of fission neutrons contributing to region 2 is effectively equal to the integral of region 2, I_2, divided by the measurement time t,

$$r_{f2} = \frac{I_2 + 1}{t} \approx \frac{I_2}{t}. \tag{14}$$

Substituting Eq. (14) into Eq. (13) to eliminate r_{f2} yields

$$r_1 = \left(r_f - \frac{I_2}{t}\right) + r_b. \tag{15}$$

Fission neutron multiplet detection theory may be used to predict the integral of region 2,

$$I_2 = N_f \sum_{i=2}^{\infty} (i-1) P_i, \tag{16}$$

where N_f is the number of fission events which occurred during the measurement, scaled by the probability to detect fission neutron multiplets of order 2 or greater weighted by the associated contribution of time intervals to region 2 by the detected fission neutron multiplets. This model holds under the assumption that detected fission neutron multiplets are sufficiently separated in time. This separation is dependent on the fission reaction rate in the source, the system absolute neutron detection efficiency, and the system average neutron dieaway time. To first order, the assumption holds if the average time spacing between Poisson events is much larger than the neutron dieaway time. The average time spacing is the average of the probability density function given in Eq. (8), given by $1/r$ where r is the average rate of Poisson events.

The number of fission events which occurred during the measurement is related to the source fission neutron yield, S_f, and average number of fission neutrons emitted per fission event, $\bar{\nu}$,

$$N_f = \frac{S_f t}{\bar{\nu}}, \tag{17}$$

where the fission neutron yield is a function of the fission neutron count rate r_f and the absolute fission neutron detection efficiency ε_f,

$$S_f = \frac{r_f}{\varepsilon_f}. \tag{18}$$

Combining Eqs. (16), (17), and (18), substituting the result into Eq. (15) to eliminate the variable I_2, and algebraically rearranging yields:

$$r_1 = r_b + r_f \left[1 - \frac{1}{\bar{\nu}\varepsilon_f} \sum_{i=2}^{\infty} (i-1) P_i\right]. \tag{19}$$

Further algebraic manipulation of this equation, using Eq. (11) to eliminate r_f and fully expanding all terms yields the FTIDA method governing equation,

$$r_1 - r_b - \left(r_{tot} - r_b\right)\left[1 - \frac{1}{\bar{\nu}\varepsilon_f} \sum_{i=2}^{\infty} (i-1) \sum_{\nu=i}^{\infty} \binom{\nu}{i} \varepsilon_f^i \left(1-\varepsilon_f\right)^{\nu-i} P(\nu)\right] = 0, \tag{20}$$

where ε_f is the single unknown. The absolute fission neutron detection efficiency is auto-calibrated by solving this equation using an algebraic root-finding algorithm.

Because Eq. (20) is implicit with respect to the absolute fission neutron detection efficiency, it is not possible to apply general uncorrelated uncertainty propagation to determine the statistical uncertainty of ε_f. Instead, a Monte Carlo method is used to evaluate the uncertainty by repeating the calculation of ε_f for a number of Gaussian statistical realizations of Eq. (20) using the statistical uncertainty of the known parameters. Details of uncertainty quantification for the FTIDA method are presented in [20].

3.4.3. The MTIDA method

The purpose of the MTIDA method is to isolate the count rates of (α,n) and fission neutrons contributing to the total count rate measured for a mixed (α,n) + fission neutron source. In measurements of such sources, the total count rate measured with the detector system, r_{tot}, is the sum of the (α,n) neutron count rate, r_α, the fission neutron count rate, r_f, and the background neutron count rate, r_b,

$$r_{tot} = r_\alpha + r_f + r_b. \tag{21}$$

The background count rate is the total count rate computed using Eq. (1) for a separate background measurement with no neutron sources in the detector system.

The fission neutron count rate is decomposed into components contributing to regions 1 and 2 of the measured time interval distribution in the same way as discussed in Section 3.4.2,

$$r_f = r_{f1} + r_{f2}, \tag{22}$$

and the initial form of the uncorrelated neutron count rate, r_1,

$$r_1 = r_\alpha + r_{f1} + r_b = r_\alpha + \left(r_f - r_{f2}\right) + r_b, \tag{23}$$

is obtained from the measured time interval distribution by fitting a single exponential function to region 1.

The theoretical prediction of r_{f2} is also performed in the same way as in the FTIDA method through the utilization of fission neutron multiplet detection theory. Substituting the theoretical form of r_{f2},

$$r_{f2} = \frac{r_f}{\bar{\nu}\varepsilon_f} \sum_{i=2}^{\infty} (i-1)\, P_i, \tag{24}$$

into Eq. (23) yields

$$r_1 = r_\alpha + r_b + r_f \left[1 - \frac{1}{\bar{\nu}\varepsilon_f} \sum_{i=2}^{\infty} (i-1)\, P_i \right]. \tag{25}$$

In Eq. (25), r_α may be eliminated as an unknown by substituting $r_\alpha = r_{tot} - r_f - r_b$, a result of Eq. (21). By performing this substitution and through algebraic manipulation of the result, it is possible to derive an explicit equation for the fission neutron count rate:

$$r_f = \frac{\bar{\nu}\varepsilon_f \left(r_{tot} - r_1 \right)}{\sum_{i=2}^{\infty} \left((i-1) \sum_{\nu=i}^{\infty} \binom{\nu}{i} \varepsilon_f^i \left(1-\varepsilon_f\right)^{\nu-i} P(\nu) \right)}. \tag{26}$$

Eq. (26) has two unknowns – ε_f and r_f – therefore requiring that the absolute fission neutron detection efficiency be known in order to compute the fission neutron count rate. The absolute fission neutron detection efficiency may be determined in a variety of ways listed below in order of descending preference:

1. Measure a pure fission neutron source of the same type as that in the mixed (α,n) + fission neutron source and apply the FTIDA method to determine ε_f.
2. Measure a ^{252}Cf source, apply the FTIDA method to obtain $\varepsilon_f^{(\text{Cf-252})}$, and use Monte Carlo simulations of the ^{252}Cf and fission source of interest spectra to relatively-calibrate the efficiency: $\varepsilon_f = \varepsilon_f^{(\text{Cf-252})} \left(\frac{\varepsilon_f}{\varepsilon_f^{(\text{Cf-252})}} \right)_{\text{MC}}$. Other methods, such as absolute neutron correlation counting or the measurement of a calibrated source, could also be used to obtain $\varepsilon_f^{(\text{Cf-252})}$.
3. Measure a ^{252}Cf source, apply the FTIDA method to obtain $\varepsilon_f^{(\text{Cf-252})}$, and assume that $\varepsilon_f \approx \varepsilon_f^{(\text{Cf-252})}$ — an accurate assumption based on results of detector system neutronics characterization shown in Table 2. Other methods, such as absolute neutron correlation counting or the measurement of a calibrated source, could also be used to obtain $\varepsilon_f^{(\text{Cf-252})}$.
4. Use Monte Carlo simulations to directly obtain an estimate of ε_f.

Once the absolute fission neutron detection efficiency is obtained, Eq. (26) is used to directly compute the fission neutron count rate r_f. The (α,n) neutron count rate may then be obtained by rearranging Eq. (21),

$$r_\alpha = r_{tot} - r_f - r_b. \tag{27}$$

Uncertainty quantification in the MTIDA method is performed by applying general uncorrelated uncertainty propagation first to Eq. (26) to obtain the fission neutron count rate statistical uncertainty, and then to Eq. (27) to obtain the (α,n) neutron count rate statistical uncertainty. This uncertainty quantification process is detailed in [20].

4. Measurements and analysis

A set of five production measurements were performed using the (α,n) neutron detector system in order to evaluate the accuracy of the detector weighting and time interval distribution analysis methods discussed in Section 3. These measurements involved three neutron sources: an Eckert & Ziegler AmBe (α,n) neutron source with a calibrated (α,n) neutron yield of S_α = 3254 ± 49 n/s, an uncalibrated 1 μCi Eckert & Ziegler ^{252}Cf spontaneous fission neutron source, and an uncalibrated, low-activity RPI ^{252}Cf source. The E&Z ^{252}Cf neutron yield was believed to be on the order of 4000 n/s and the RPI ^{252}Cf neutron yield was believed to be on the order of 400 n/s. Table 6 contains a listing of the measurements and their method validation objectives. All measurements were performed using the typical ^{3}He detector operating parameters given in Table 3 with cycle lengths of 15 min.

Table 6
Production measurement characteristics.

Measurement	Number of cycles	Methods evaluated
Background	480	–
AmBe	192	Detector weighting
E&Z ^{252}Cf	192	Detector weighting FTIDA
AmBe + E&Z ^{252}Cf	115	Detector weighting MTIDA
AmBe + RPI ^{252}Cf	192	Detector weighting MTIDA

The five measurements consisted of a background measurement, measurements of the AmBe (α,n) and E&Z ^{252}Cf spontaneous fission neutron sources individually, and measurements of the AmBe + E&Z ^{252}Cf and AmBe + RPI ^{252}Cf sources together. The purpose of the background measurement was to obtain neutron background count rates for each of the 96 ^{3}He detectors in the system. These background count rates were used to background-correct the measured data obtained in the remaining neutron source measurements.

The purpose of the AmBe source measurement was to evaluate the accuracy of the weighting method by comparing the neutron yield computed using the weighting analysis to the AmBe source calibrated neutron yield. This comparison is valid only because the AmBe source is a pure (α,n) neutron source. For the detector weighting analysis of the AmBe source measurement, the weights given in Section 3.3 were utilized.

The purpose of the E&Z ^{252}Cf source measurement was to evaluate the relative accuracy of the weighting and FTIDA methods in determining the total (spontaneous fission) neutron yield of a pure fission source through cross comparison of the method results. Given that the E&Z ^{252}Cf neutron yield was not calibrated, absolute evaluation of the detector weighting and FTIDA methods was not possible in this case. From the measured data, the fission neutron yield was computed using the detector weighting method as well as using the fission neutron count rate and the auto-calibrated absolute fission neutron detection efficiency obtained using the FTIDA method,

$$S_f = \frac{r_f}{\varepsilon_f}. \tag{28}$$

This comparison is valid only because the ^{252}Cf source is a pure spontaneous fission neutron source. The detector weighting analysis utilized the weights given in Section 3.3, and the FTIDA method utilized the Santi & Miller prompt fission neutron multiplicity distribution for ^{252}Cf spontaneous fission [24].

The purpose of the remaining two mixed (α,n) + fission source measurements was to evaluate the accuracy of the detector weighting and MTIDA methods, used together, to determine the (α,n) neutron yield of a mixed neutron source. The (α,n) neutron yield of the mixed source was computed by first determining the total neutron yield using the weighting method ($S = S_\alpha + S_f$) and then subtracting the fission neutron contribution obtained from the MTIDA method ($S_f = \frac{r_f}{\varepsilon_f}$) to obtain S_α:

$$S_\alpha = S - S_f = S - \frac{r_f}{\varepsilon_f}. \tag{29}$$

The computed (α,n) neutron yields were compared to the calibrated AmBe neutron yield to evaluate the method accuracy. The analysis utilized the weights given in Section 3.3 and the absolute fission

Table 7
Background- and deadtime-corrected response function data obtained from the four neutron source validation measurements.

Ring number	Response Value [cps/detector]			
	AmBe	E&Z ^{252}Cf	AmBe +E&Z ^{252}Cf	AmBe +RPI ^{252}Cf
1	16.5 ± 0.010	29.3 ± 0.023	45.4 ± 0.023	19.3 ± 0.012
2	18.0 ± 0.010	30.8 ± 0.024	48.9 ± 0.024	20.9 ± 0.013
3	16.9 ± 0.010	26.6 ± 0.022	43.8 ± 0.022	19.3 ± 0.012
4	13.7 ± 0.009	19.2 ± 0.019	33.1 ± 0.019	15.4 ± 0.011
5	10.4 ± 0.008	12.5 ± 0.016	23.1 ± 0.016	11.5 ± 0.009
6	7.0 ± 0.006	7.2 ± 0.013	14.3 ± 0.013	7.7 ± 0.008
7	4.5 ± 0.005	4.0 ± 0.010	8.6 ± 0.010	4.9 ± 0.006

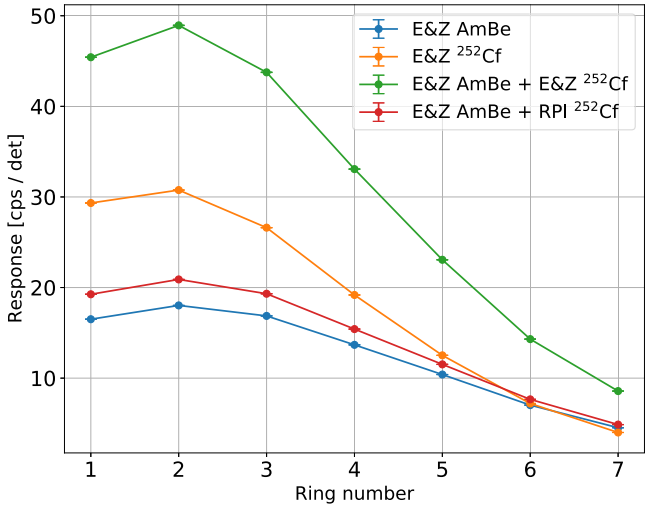

Fig. 12. Background- and deadtime-corrected response functions obtained from the four neutron source validation measurements.

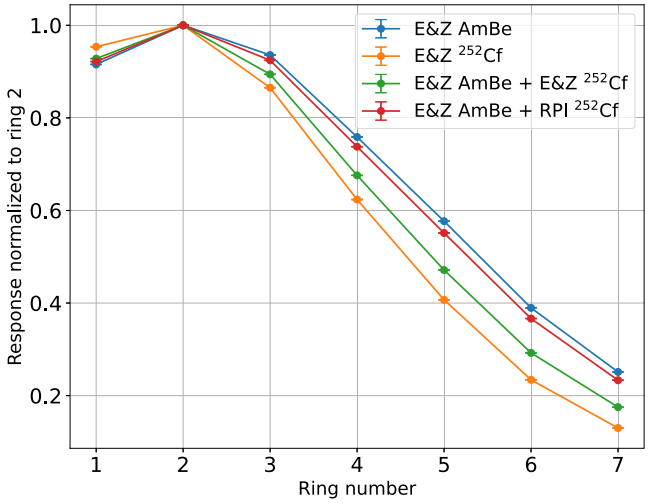

Fig. 13. Background- and deadtime-corrected response functions obtained from the four neutron source validation measurements, normalized to ring 2. Note that as average source neutron energy increases, the response functions tilt to increased rates in the outer detector rings due to the increased mean free path of the neutrons in the system.

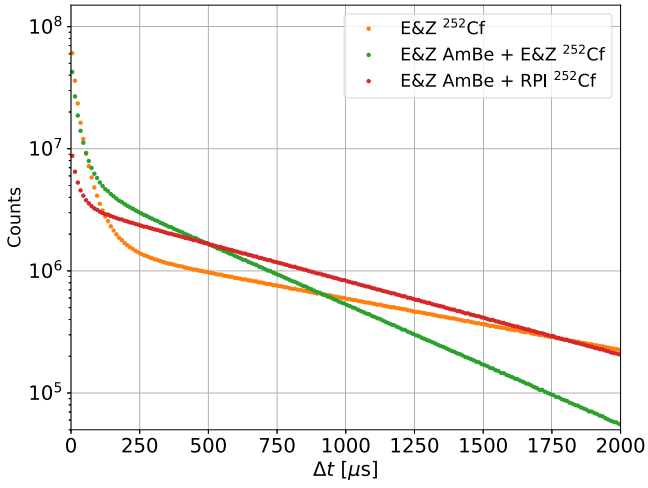

Fig. 14. Time interval distributions measured for the three neutron source validation measurements involving correlated ^{252}Cf spontaneous fission neutron detection.

neutron detection efficiency obtained via the FTIDA method analysis of the E&Z ^{252}Cf measurement. The purpose of performing two mixed source measurements was to test the weighting + MTIDA method for different α ratios of source (α,n) vs. fission neutrons. In the case of the E&Z sources the neutron emission is slightly dominated by fission neutrons ($\alpha < 1$)whereas in the case of the E&Z AmBe and RPI ^{252}Cf sources the total neutron yield is comprised of only roughly 10% fission neutrons ($\alpha \approx 10$).

The raw measured data for all five measurements was inspected for errors (e.g. serial data transfer issues, serial port buffer overruns,^{3}He count rate instability) and the pulse height distribution alignment for all detectors in each ring was verified. Measured data was corrected for deadtime and neutron background. The response functions for the four neutron source measurements were then computed, as well as the time interval distributions for the three measurements involving ^{252}Cf. The response function values are tabulated in Table 7 and are plotted both in raw form in Fig. 12 and normalized to ring 2 in Fig. 13. The time interval distributions, computed with a bin width of 10 μs, are shown in Fig. 14 up to time intervals of 2 ms.

Fig. 12 shows that the four measured response functions generally have the same shape, peaking in the second ring of ^{3}He detectors and then monotonically decreasing as the ring radius increases. The peak lies in the second ring due to the strong thermal neutron absorption occurring close to the first ring of detectors by the cadmium thermal neutron filter. Energy spectrum dependence of the response functions is visually evident, as the response for the E&Z ^{252}Cf measurement exhibits a larger difference between the response in the inner and outer ring as compared to the three other measurements. This is due to the fact that the ^{252}Cf spontaneous fission PFNS is significantly softer than the AmBe (α,n) spectrum.

The time interval distributions plotted for the three measurements involving ^{252}Cf, shown in Fig. 14, exhibit the expected features that are utilized by the FTIDA and MTIDA coincidence methods. The region 1 slopes of the distributions are proportional to the total neutron yield of the source, as the time interval distributions of the sources sorted by increasing total neutron yield — E&Z ^{252}Cf, E&Z AmBe + RPI ^{252}Cf, E&Z AmBe + E&Z ^{252}Cf — follow this trend. The region 2 area of the time interval distributions relative to the total distribution integral also follows the expected trend of inverse proportionality to the fraction of source neutrons which are fission neutrons. This expected behavior

Table 8
Production measurement analysis results.

	AmBe	E&Z ^{252}Cf	AmBe + E&Z ^{252}Cf	AmBe + RPI ^{252}Cf
Count Rate	r_α = 1300.0 ± 0.3 cps	r_f = 1984.0 ± 0.5 cps	r_{tot} = 3291.0 ± 0.8 cps	r_{tot} = 1482.7 ± 0.4 cps
Region 1 Fit Slope	–	r_1 = 968.4 ± 0.2 s^{-1}	r_1 = 2265.9 ± 1.5 s^{-1}	r_1 = 1390.4 ± 0.4 s^{-1}
Assumed Efficiency	–	–	ε_f = 48.3%	ε_f = 48.3%
Detector Weighting Results	S = 3255 ± (38 + 44[a]) n/s	S = 4141 ± (50 + 56[a]) n/s	S = 7376 ± (82 + 100[a]) n/s	S = 3620 ± (46 + 49[a]) n/s
FTIDA Results	–	ε_f = 0.4833 ± 0.0014 S_f = 4105 ± 12 n/s	–	–
MTIDA Results	–	–	r_α = 1289.2 ± 15.0 cps r_f = 2001.8 ± 15.0 cps	r_α = 1296.5 ± 2.0 cps r_f = 186.2 ± 2.0 cps
(α,n) Neutron Yield	S_α = 3255 ± (38 + 44[a]) n/s	–	S_α = 3234 ± (89 + 100[a]) n/s	S_α = 3235 ± (46 + 49[a]) n/s
Estimated (α,n) Neutron Detection Efficiency	39.9%	–	40.1%	40.1%

[a]Contribution of the detector weighting method systematic uncertainty.

is leveraged in the coincidence methods to isolate and correct for the fission neutron contribution to the measurements during data analysis.

5. Results

The results of the production measurement analyses discussed in Section 4 are given in Table 8. Detector weighting analysis of the AmBe source measurement was found to be very accurate, as shown in Table 8, determining a total neutron yield of 3255 ± 82 n/s for the AmBe source. Given that the AmBe source is a pure (α,n) source, this value was compared directly to the AmBe source calibrated neutron yield of 3254 ± 49 n/s — a difference of 0.04%. While the true accuracy of the weighting method cannot be known to better than the calibration uncertainty of 1.5%, the agreement between these values is encouraging in validating the performance of the detector weighting method.

Although the results of the FTIDA and detector weighting analyses of the E&Z ^{252}Cf source measurement could not be compared to a calibrated value, the method accuracy was relatively evaluated by through cross comparison. An absolute fission neutron detection efficiency for ^{252}Cf spontaneous fission of 0.4833 ± 0.0014 was determined using the FTIDA method, corresponding to a fission neutron yield of 4105 ± 12 n/s via Eq. (28) and the background- and deadtime-corrected fission neutron count rate obtained from the measurement and given in Table 8. The detector weighting method computed a total (spontaneous fission) neutron yield of 4141 ± 106 n/s for the source. These values agree to within 1%, which is excellent relative agreement between the two methods and provides another level of validation of the weighting and FTIDA methods.

The most challenging analysis in this work was the analysis of the two (α,n) + fission neutron source measurements which utilized the combination of the weighting and MTIDA methods to obtain the (α,n) neutron yield of the mixed source. For the measurement of the E&Z AmBe and ^{252}Cf sources, the MTIDA method separated the total count rate into an (α,n) neutron contribution of r_α = 1289 ± 15.0 cps and a fission neutron contribution of r_f = 2001.8 ± 15.0 cps. Comparing these values to the count rates obtained in the measurements of the E&Z sources individually, the MTIDA method successfully separated the count rates to an accuracy of better than 1% for both neutron types.

Using the weighting method to compute the total neutron yield of the E&Z AmBe + E&Z ^{252}Cf source and correcting the total neutron yield for the fission neutron contribution via MTIDA results and Eq. (29), an (α,n) neutron yield of 3234 ± 189 n/s was obtained for the mixed source condition. While the (α,n) neutron yield was again found to be very accurate, agreeing with the AmBe source calibrated value to 0.6%, the total uncertainty of the (α,n) neutron yield was quite large. The uncertainty can be decreased by performing a longer measurement to reduce the statistical uncertainty component, but it is important to note that the magnitude is exacerbated for cases such as this where there is a large fission neutron correction. In this case, the total neutron yield is large relative to the (α,n) neutron yield, and the systematic uncertainty of the total neutron yield is transferred directly from S to S_α via Eq. (29) (see Table 8). As a result, the total uncertainty increases for measurements of sources which are dominated by fission neutron emission.

The same analysis approach was taken for the second mixed neutron source measurement of the E&Z AmBe source + the RPI ^{252}Cf source — however, in this case, the neutron emission was dominated by (α,n) neutrons. As shown in Table 8, the MTIDA method was again able to very accurately separate the (α,n) and fission neutron count rates, computing an (α,n) neutron count rate of 1296.5 ± 2.0 cps which agrees to 0.3% of the value obtained from the AmBe source measurement. Using the same procedure to compute the total neutron yield using the detector weighting method and correct for the fission neutron contribution, an (α,n) neutron yield of 3235 ± 95 n/s was determined for the mixed source. This result is accurate to the AmBe calibrated neutron yield to 0.6%, and the analysis demonstrates the concept that the systematic uncertainty in the final (α,n) neutron yield is reduced for cases where (α,n) neutrons dominate the source neutron emission (large α).

6. Conclusions

In this work, a neutron detection system and data analysis methods were developed for (α,n) neutron counting of enriched uranium compounds with low total neutron emission rate to support validation needs for (α,n) reaction nuclear data and (α,n) neutron source modeling techniques. The detection system, a moderated ^{3}He detector array with digital data acquisition, was successfully designed, manufactured, and operated using feature-rich data acquisition software developed and tested in-house. The high-fidelity digital neutron detection event data was processed, corrected, and analyzed using total neutron counting and coincidence methods developed as part of this work. Through measurements of a calibrated AmBe (α,n) neutron source and multiple ^{252}Cf neutron sources with varying spontaneous fission neutron yields, the accuracy of the total neutron counting and coincidence methods was validated both independently and jointly. It was found that in three measurements, one measurement of the pure AmBe (α,n) source and two experiments measuring the AmBe source with different ^{252}Cf spontaneous fission sources to include fission neutron contamination, the methods were able to deduce the (α,n) neutron yield from the measured data to an accuracy better than 1% in all cases.

The foremost future work topic for this detector system and data analysis methods is the improvement of the detector weighting method energy grid selection process and the calculation of the detector weights. While careful evaluation procedures were taken in this work to select the energy grid, the development of a more rigorous process, potentially utilizing optimization techniques such as principal component analysis to precisely identify an optimal energy grid, are advantageous. Additionally, exploration of methods to intelligently constrain the least-squares solution to encourage weights with smaller magnitude without adding significant bias and introducing degradation of performance is of interest for reduction of weighting method statistical uncertainty. For example, regularization methods such as ridge regularization [25] operate in this way when applied to linear least squares, but initial testing of the weighting method utilizing this regularization scheme were found that the regularization introduced a large bias into the calculations.

Declaration of competing interest

The authors declare that they have no known competing financial interests or personal relationships that could have appeared to influence the work reported in this paper.

Data availability

The data that has been used is confidential.

Acknowledgments

The authors would like to acknowledge Dr. Robert Block, Dr. Devin Barry, Dr. Amanda Lewis, and Brian Epping who were all instrumental in the technical and administrative progression of this project. In addition, the contributions of current/former RPI Gaerttner Linear Accelerator technical staff Matt Gray, Larry Krusieski, John Fava, Edwin Frank, and Brian Martindale were critical to completing the detector system design and manufacturing.

Funding

This work was supported by Naval Nuclear Laboratory, United States.

References

[1] J. Sprinkle, Total neutron counting instruments and applications, in: Passive Nondestructive Assay of Nuclear Materials, 1991, Los Alamos National Laboratory report LA-UR-90-732.

[2] Radioactive neutron sources emission rates, 2014, National Institute of Standards and Technology report RPD-P-13. URL https://www.nist.gov/system/files/documents/pml/div682/Procedure13v405.pdf.

[3] H. Menlove, Neutron coincidence instruments and applications, in: Passive Nondestructive Assay of Nuclear Materials, 1991, Los Alamos National Laboratory report LA-UR-90-732.

[4] C. Vincent, The pulse separation spectrum for the detection of neutrons from a mixture of fissions and single-neutron events, Nucl. Instrum. Methods 138 (1976) 261–266.

[5] C. Vincent, The detection of groups of associated pulses in a train otherwise comprised of randomly timed single pulses, Nucl. Instrum. Methods 158 (1979) 181–184.

[6] D. Reilly, N. Ensslin, H. Smith Jr., S. Kreiner, Passive Nondestructive Assay of Nuclear Materials, Los Alamos National Laboratory, Los Alamos NM, 1991, Los Alamos National Laboratory report LA-UR-90-732.

[7] N. Ensslin, W. Harker, M. Krick, D. Langner, M. Pickrell, J. Stewart, Application guide to neutron multiplicity counting, 1998, Los Alamos National Laboratory report LA-13422-M.

[8] P. Baeten, M. Bruggeman, Neutron coincidence counting based on time interval analysis with one and two dimensional rossi-alpha distributions: An application for passive neutron waste assay, Tech. rep., 1996, SCK CEN report BLG-711.

[9] K. Kim, L. Nakae, M. Prasad, N. Snyderman, J. Verbeke, Fission chain restart theory, Nucl. Sci. Eng. 188 (2017) 57–84.

[10] D. Chambers, J. Chandrasekaran, S. Walston, Fourier method for calculating fission chain neutron multiplicity distributions, Nucl. Sci. Eng. 184 (2016) 244–253.

[11] M. Prasad, N. Snyderman, Statistical theory of fission chains and generalized Poisson neutron counting distributions, Nucl. Sci. Eng. 172 (2012) 300–326.

[12] M. Prasad, N. Snyderman, J. Verbeke, R. Wurtz, Time interval distributions and the rossi correlation function, Nucl. Sci. Eng. 174 (2013) 1–29.

[13] M. Prasad, N. Snyderman, S. Walston, Neutron time interval distributions with background neutrons, Nucl. Sci. Eng. 186 (2017) 277–292.

[14] J. Stewart, H. Menlove, D. Mayo, W. Geist, L. Carrillo, G. Herrera, The epithermal neutron multiplicity counter design and performance manual: More rapid plutonium and inventory verifications by factors of 5-20, 2000, Los Alamos National Laboratory report LA-13743-M.

[15] S. Croft, D. Henzlova, Determining ^{252}Cf source strength by absolute passive neutron correlation counting, Nucl. Instrum. Methods Phys. Res. A 714 (2013) 5–12.

[16] C. Romano, T. Ault, L. Bernstein, R. Bahran, B. Rearden, P. Talou, B. Quiter, S. Pozzi, M. Devlin, J. Burke, T. Bredeweg, E. Mccutchan, S. Stave, T. Bailey, S. Hogle, C. Chapman, A. Hurst, N. Nelson, F. Tovesson, D. Hornback, Proceedings of the nuclear data roadmapping and enhancement workshop (NDREW) for nonproliferation, Tech. rep., 2018, Oak Ridge National Laboratory report ORNL/LTR-2018/510.

[17] C. Romano, D. Brown, S. Croft, A. Favalli, L. Nakae, M. Pigni, S. Skutnik, M. Smith, W. Wieselquist, M. Zerkle, (α,N) nuclear data scoping study, Tech. rep., 2020, Oak Ridge National Laboratory report ORNL/TM-2020/1789.

[18] D. Griesheimer, A. Pavlou, J. Thompson, J. Holmes, M. Zerkle, E. Caro, H. Joo, In-line (α,n) source sampling methodology for Monte Carlo radiation transport simulations, Nucl. Eng. Technol. 49 (2017) 1199–1210.

[19] D. Brown, M. Chadwick, R. Capote, A. Kahler, A. Trkov, W. Herman, A. Sonzogni, Y. Danon, A. Carlson, M. Dunn, D. Smith, G. Hale, G. Arbanas, R. Arcilla, C. Bates, B. Beck, B. Becker, F. Brown, R. Casperson, J. Conlin, D. Cullen, M. Descalle, R. Firestone, T. Gaines, K. Guber, A. Hawari, J. Holmes, T. Johnson, T. Kawano, C. Kiedrowski, A. Koning, S. Kopecky, L. Leal, J. Lestone, C. Lubitz, J. Marquez, C. Mattoon, E. McCutchan, S. Mughabghab, P. Navratil, D. Neudecker, G. Nobre, G. Noguere, M. Paris, M. Pigmi, A. Plompen, B. Pritychenko, V. Pronyaev, D. Roubtsov, D. Rochman, P. Romano, P. Schillebeeckx, S. Simakov, M. Sin, I. Sirakov, B. Sleaford, V. Sobes, S. Soukhovitskii, I. Stetcu, P. Talou, I. Thompson, S. van der Marck, S. Welser-Sherrill, D. Wiarda, M. White, J. Wormald, R. Wright, M. Zerkle, G. Aerovnik, Y. Zhu, ENDF/B-VIII.0: The 8th major release of the nuclear reaction data library with CIELO-project cross sections, new standards and thermal scattering data, Nucl. Data Sheets 148 (2018) 1–142.

[20] A. Ney, Development of Experimental and Analytical Methods for Low-Rate (α,n) Neutron Source Characterization (Ph.D. thesis), Rensselaer Polytechnic Institute, Troy, NY, 2022, https://hdl.handle.net/20.500.13015/6264.

[21] C. Werner, J. Bull, C. Solomon, F. Brown, G. McKinney, M. Rising, D. Dixon, R. Martz, H. Hughes, L. Cox, A. Zukaitis, J. Armstrong, R. Forster, L. Casswell, MCNP version 6.2 release notes, Tech. rep., Los Alamos National Laboratory, Los Alamos NM, 2018, Los Alamos National Laboratory report LA-UR-18-20808.

[22] W. Wilson, R. Perry, E. Shores, W. Charlton, T. Parish, G. Estes, T. Brown, E. Arthur, M. Bozoian, T. England, D. Madland, J. Stewart, SOURCES 4C: A code for calculating (alpha,n), spontaneous fission, and delayed neutron sources and spectra, 2002, Los Alamos National Laboratory report LA-UR-02-1839.

[23] G. Knoll, Radiation Detection and Measurement, fourth ed., John Wiley & Sons, Inc., Hoboken, NJ, 2010.

[24] P. Santi, M. Miller, Reevaluation of prompt neutron emission multiplicity distributions for spontaneous fission, Nucl. Sci. Eng. 160 (2) (2008) 190–199.

[25] A. Hoerl, R. Kennard, Ridge regression: Biased estimation for nonorthogonal problems, Technometrics (2000).